Available online at www.sciencedirect.com
ScienceDirect
Trans. Nonferrous Met. Soc. China 24(2014) 2459−2467
Transactions of Nonferrous Metals Society of China
www.tnmsc.cn

Fatigue crack growth behaviour of friction stir welded AA7075-T651 aluminium alloy joints

P. SIVARAJ, D. KANAGARAJAN, V. BALASUBRAMANIAN

Department of Manufacturing Engineering, Annamalai University, Annamalai Nagar, Tamil Nadu 608002, India

Received 24 September 2013; accepted 12 June 2014

Abstract: The aim of the present work is to evaluate the fatigue crack growth behaviour of 12 mm thick AA 7075-T651 aluminium alloy plates joined by FSW. Fatigue crack growth test was carried out on center cracked tensile (CCT) specimens extracted from the FSW joints and unwelded parent metal. Transverse tensile properties of the unwelded parent metal and welded joints were evaluated. Microstructures of the welded joints were analyzed using optical microscopy and transmission electron microscopy. The scanning electron microscope was used to characterize the fracture surfaces. It was found that the ΔK_{cr} of the welded joint is reduced by 10×10^{-3} MPa·m$^{1/2}$ in comparison with the unwelded parent metal. Hence, the fatigue life of the friction stir welded AA 7075-T651aluminium alloy joints is appreciably lower than that of the unwelded parent metal, which is attributed to the dissolution of precipitates in the weld region during friction stir welding.

Key words: AA 7075 aluminium alloy; friction stir welding; fatigue crack growth; microstructure

1 Introduction

High-strength, precipitation-hardenable 7000-series aluminium alloys, such as alloy AA 7075, are used extensively in military and aircraft primary structures [1]. This alloy derives its strength from precipitation of Mg_2Zn and Al_2CuMg phases. The assembly of metals has been a fundamental topic for many years. Major problem with this alloy is that, it is not fusion weldable. In particular, this class of aluminium alloy is difficult to join by conventional fusion welding practices because the dendritic structure formed in the fusion zone can seriously deteriorate the mechanical properties of the joint. It is extremely sensitive to weld solidification cracking as well as heat-affected zone (HAZ) liquation cracking due to the presence of copper. Though, it is possible to overcome the problem of weld solidification cracking using a suitable non heat-treatable aluminium alloy filler (such as Al−Mg or Al−Si), the resulting joint efficiencies are appreciably lower [2].

Friction stir welding (FSW), a solid state joining process developed by The Welding Institute (TWI), UK, has emerged as a promising process with the potential to join aluminium alloys which are traditionally considered unweldable. FSW is well suited for joining aluminum alloys, especially those that are typically considered to be unweldable, such as 2xxx and 7xxx series aluminum alloys [3]. The benefits of FSW are: 1) capability to weld difficult-to-weld aluminium alloys, 2) fewer weld defects, 3) better dimensional stability of the welded structure and possibility to weld linear and contour welding. Although the weld material remains in the solid state throughout the joining process, it is exposed to a high temperature extrusion [4,5] and experiences high levels of deformation [6], leading to significant modification of the microstructure and mechanical properties coupled with development of significant levels of residual stress [7]. For the aircraft components fatigue performance was known to be one of the crucial assessment qualities, therefore many efforts have been done to investigate the fatigue properties of friction stir welded various grades of aluminium alloy joints.

HASSAN et al [8] studied the stability of nugget zone grain structures in high strength Al alloy friction stir welds during solution treatment and reported that weld nugget zone grain structures were inherently unstable in high strength aluminum alloy AA7010 and abnormal grain growth (AGG) occurred in entire weld nugget zone (WNZ) due to the dissolution of soluble precipitates during ST at 475 °C. MOREIRA et al [9] conducted fatigue crack growth in friction stir welds of 6082-T6

Corresponding author: P. SIVARAJ; Tel: +91-4144-239734 (O); Fax: +91-4144-239734/238275; E-mail: cemajorsiva@gmail.com
DOI: 10.1016/S1003-6326(14)63371-9

and 6061-T6 aluminium alloys and the results were compared with the unwelded parent metal. The results showed that the crack propagation rates of the friction stir welded material are lower than the crack propagation rates of unwelded parent metal.

The effects of three welding processes on fatigue crack growth resistance of gas tungsten arc, electron beam and friction stir welded joints of AA2219 aluminium alloy were studied by MALARVIZHI and BALASUBRAMANIAN [10]. The results showed that the FSW joints exhibited superior tensile and fatigue properties compared with EBW and GTAW joints. CHEN et al [11] investigated the effects of precipitates on the fatigue crack growth rate of AA7055 Al alloy subjected to different aging treatments using transmission electron microscope and fatigue crack growth testing. The results showed that the T77 treated samples exhibited the lowest crack growth rate, while the crack growth rate of over-aged samples was the highest.

ZHAO and JIANG [12] conducted fatigue test on AA 7075−T651 aluminium alloy under uniaxial, torsion and axial-torsion loading conditions and gave a fatigue model which can predict the fatigue life for most experiments. ZHOU et al [13] investigated the fatigue life of friction stir welded 10 mm thick plates of aluminium alloy 5083. It was reported that the fatigue life was found to be 9−12 times longer than that of MIG-pulse welds under R=0.1 and the fatigue characteristic value of each welds has been increased from 39.8 MPa for MIG to 67.3 MPa for FSW. CAVALIERE et al [14] investigated tensile and fatigue properties of 4 mm thick 2198 Al−Li alloy friction stir welded sheets. SRIVATSAN et al [15] evaluated the fracture behavior of aluminium alloy 7055 parent material. The tensile properties, microhardness, microstructure and fracture surface morphology of the GMAW, GTAW and FSW joints of RDE 40 aluminium alloy were evaluated and the results were compared by LAKSHMINARAYANAN and BALASUBRAMANAIAN [16]. From the literature review, it is understood that most of the published works have focused on tensile properties and microstructural characterization of friction stir welded AA7075 aluminium alloy. Hence, the present investigation is aimed to study the fatigue crack growth behaviour of 12 mm thick plates of AA7075-T651 aluminium alloy butt joints made by FSW process and the resultant fatigue crack growth properties are compared with the unwelded fatigue crack growth properties of parent metal.

2 Experimental

Rolled plates of 12 mm thick aluminium alloy (AA 7075 in T651 condition) were used in this investigation. The chemical composition of parent metal is presented in Table 1. Figures 1(a) and (b) represent the FSW tool diagram and tool photograph respectively. Prior to welding, the abutting faces of the plates were finely milled in order to avoid surface scaling intruded with the tool. The FSW tool with tapered threaded pin profile of shoulder diameter of 36 mm, pin diameter of 12 mm and pin length of 11.6 mm was used in this study. Few trial experiments were made to identify the parameters which give the defect-free welds and those parameters were

Table 1 Chemical composition of parent metal (mass fraction, %)

Zn	Mg	Cu	Fe	Si	Mn	Cr	Ti	Al
6.1	2.9	2.0	0.50	0.4	0.30	0.28	0.20	Bal.

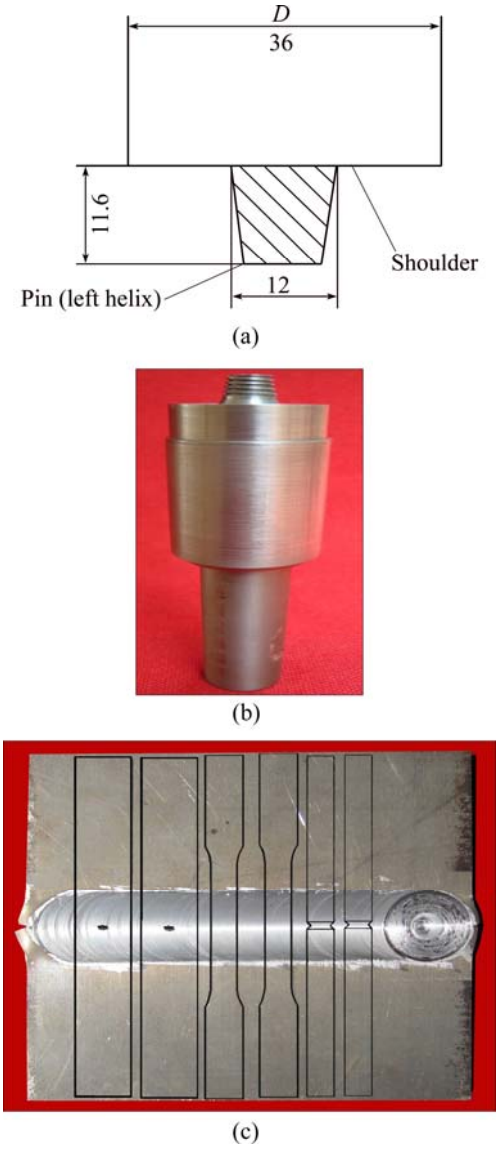

Fig. 1 Dimensions of FSW tool and joints: (a) FSW tool diagram (unit: mm); (b) FSW tool photograph; (c) Scheme of specimen extraction from fabricated joint

taken as the optimized welding parameters in this investigation. Tool rotation and welding speeds were taken as 250 r/min 25 mm/min, respectively. Necessary care was taken to avoid joint distortion during welding. The welding was carried out normally to the rolling direction of the parent metal. Figure 1(c) shows the scheme of specimen extraction plan and fabricated joint photographs respectively.

The welded joint was sliced using power hacksaw and then machined to the required dimensions. Two different tensile specimens were prepared as the ASTM E8M-04 standard guidelines. The unnotched and notched tensile specimens were prepared as shown in Figs. 2(a) and (b) respectively to evaluate yield strength, tensile strength, elongation and notch tensile strength. Tensile testing was carried out using 100 kN, electro mechanical controlled universal testing machine (Make: FIE-Blue star, India; Model: UNITEK-94100). The 0.2% offset yield strength was derived from the load displacement curve. Centre cracked tension (CCT) fatigue crack growth test specimens were prepared to the dimensions shown in Fig. 2(c) to evaluate the fatigue crack growth resistance of the weld joints. The slices derived from the friction stir welded joints were reduced to a thickness of 10 mm by shaping and grinding processes to obtain flat and required surface roughness. Then the sharp notch was machined in the weld metal region to the required length using the wire cut electric- discharge machine (EDM). Procedures prescribed by the ASTM E647−04 standard were followed for the preparation of the CCT specimens. The fatigue crack growth experiments were conducted at four different stress levels (50, 75, 100 and 125 MPa) and all the experiments were conducted under uniaxial tensile loading condition (Tension−Tension, R=stress ratio, $\sigma_{min}/\sigma_{max}$=0.1, Frequency=10 Hz) using servo hydraulic fatigue testing machine (Make: INSTRON, UK; Model: 8801) under constant amplitude loading. Before loading, the specimen surface was polished using metallographic procedures and

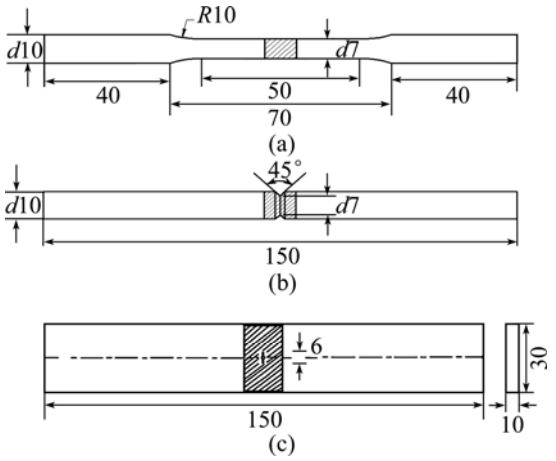

Fig. 2 Dimensions of samples used for testing (unit: mm): (a) Dimensions of un-notched tensile specimens; (b) Dimensions of notched tensile specimens; (c) Dimensions of fatigue crack growth specimen

illuminated suitably to enable the crack growth measurement. A traveling microscope (Make: MITUTOYA; Model: 5010) attached with a web camera and video output was used to monitor the crack growth with an accuracy of 0.01 mm. In this investigation, the applied stress cycle was in the tensile mode (the minimum stress was kept at $0.1p_{max}$) as the compressive mode usually closes the fatigue crack. The data points measured with an accuracy of 0.01 mm were fitted with a smooth curve in the form of crack length vs number of cycles (a vs N). Figures 3(a) and (b) show the photographs of parent metal CCT specimens before and after testing. Figures 3(c) and (d) show the photographs of FSW joint CCT specimens before and after testing.

Hardness measurement was done across the weld center line by a Vickers microhardness tester (SHIMADZU, Japan; Model: HMV-2T) with 0.49 N load and 15 s dwell time. The specimen for metallographic examination was sectioned to the required sizes from the joint regions and polished using

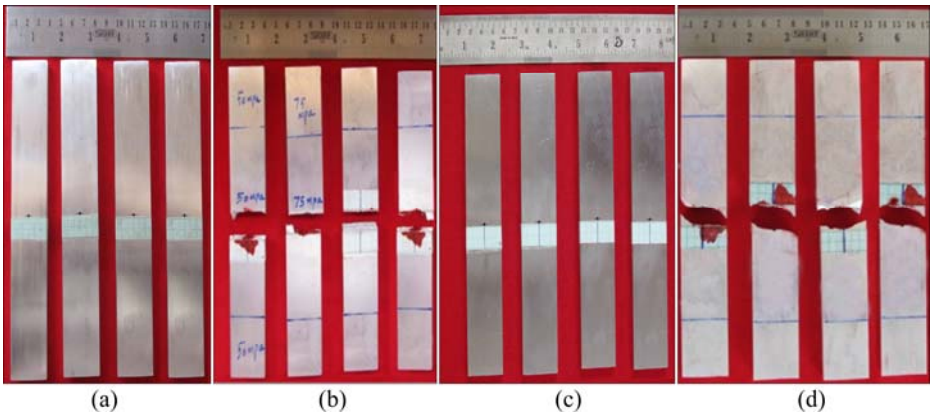

Fig. 3 Photographs of CCT specimen: (a) Parent metal before testing; (b) Parent metal after testing; (c) Weld joint before testing; (d) Weld joint after testing

different grades of emery papers. Final polishing was done using the diamond compound (1 μm particle size) in the disc polishing machine. Metallographic specimens were prepared by standard metallographic technique and were etched with Keller's reagent (150 mL H_2O, 3 mL HNO_3 and 6 mL HF). The etching solution was cooled to 0 °C and specimens were etched for about 20 s in order to study the grain structure of the weld zones and to allow for optical microscopy characterizations revealing the macro and microstructure. The microstructural analysis was done using an optical microscope (MEIJI, Japan; Model: ML7100) and a transmission electron microscope (TEM). The high resolution scanning electron microscope (HRSEM) was used to identify the mode of fracture.

3 Results

3.1 Fatigue crack growth results

The measured variation in crack length ($2a$) and the corresponding number of cycles (N) endured under the action of particular applied stress range were plotted in Fig. 4 for parent metal and FSW joint. The fracture mechanics based Paris power equation [17], was used to analyze the experimental results.

$$da/dN=C(\Delta K)^m \quad (1)$$

where da/dN is the crack growth rate; ΔK is the stress intensity factor (SIF) range; C and m are constants.

The SIF value was calculated for different values of growing fatigue crack length '$2a$' using the following expression [18]:

$$\Delta K = \phi(\Delta\sigma)\pi^{1/2}a \quad (2)$$

However, the geometry factor 'ϕ' for the CCT specimen was calculated using the expression given as

$$\phi=F(\alpha)=\sec(\alpha/2) \quad (3)$$

where $\alpha=a/W$ is crack length to specimen width ratio.

The crack growth rate, da/dN for the propagation stage, was calculated for steady state growth regime, at different intervals of crack length increment, against the associated number of cycles to propagation, as explained in the earlier section. The relationship between SIF range and the corresponding crack growth rate in terms of the best fit lines is shown in Fig. 5 for the parent metal and FSW joint. The data points plotted in the graph mostly correspond to the second stage of Paris sigmoidal relationship (10^{-6} to 10^{-3} mm/cycle). The exponent m, which is the slope of the line on lg–lg plot and the intercept 'C' of the line, were determined and shown in Table 3. At higher crack growth rate, around 10^{-3} mm/cycle, the unstable crack growth occurred and hence

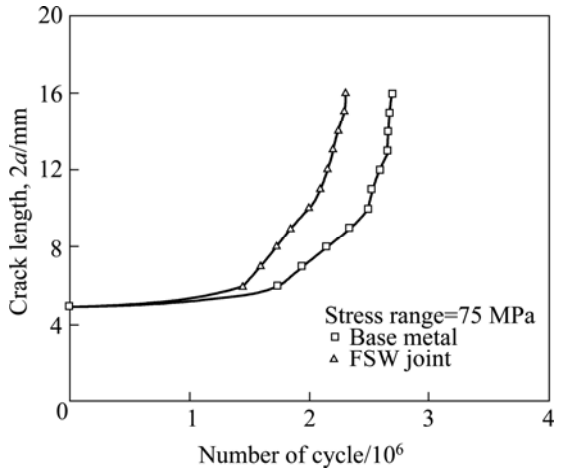

Fig. 4 Crack growth curves

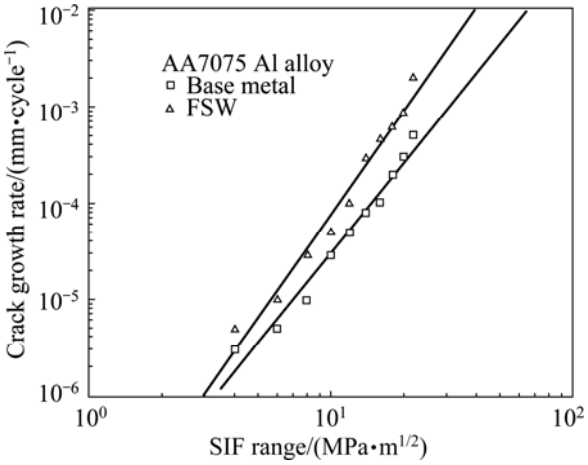

Fig. 5 Relationship between crack growth rate and SIF range

corresponding ΔK value was taken as critical SIF range (ΔK_{cr}). At lower crack growth rate, below 10^{-6} mm/cycle, the crack growth was found to be dormant and hence the corresponding ΔK was taken as threshold SIF (ΔK_{th}). The values of ΔK_{cr} and ΔK_{th} for parent metal and FSW joints were evaluated and presented in Table 2.

Table 2 Fatigue crack growth parameters of parent metal and welded joint

Specimen	Crack growth exponent m	Intercept C	Threshold SIF, ΔK_{th}/ (10^{-6}MPa·m$^{1/2}$)	Critical SIF, ΔK_{cr}/ (10^{-3}MPa·m$^{1/2}$)
Parent metal	3.09	2.32×10^{-8}	3.5	30
FSW joint	3.55	7.51×10^{-8}	3.0	20

The crack growth exponent m, which was derived from the relationship existing between crack growth rate (da/dN) and SIF range, is an important parameter to evaluate the fatigue crack growth behaviour of materials

since it decides the fatigue crack propagation life of the materials [19]. The fatigue crack growth exponent of unwelded AA7075 aluminium alloy is 3.09. The FSW joint exhibited high fatigue crack growth exponent value. The fatigue crack growth exponent of FSW joint is 3.55 which is approximately 13% higher than that of parent metal. If the fatigue crack growth exponent is larger, then the crack growth rate will be faster and the corresponding fatigue life will be lower.

3.2 Tensile properties

The transverse tensile properties such as yield strength, tensile strength and elongation of AA 7075 alloy joints were evaluated. In each condition, three specimens were tested, and the average of three results is presented in Table 3. The yield strength and tensile strength of the unwelded parent metal are 510 MPa and 563 MPa respectively. But the yield strength and tensile strength of FSW joint are 335 MPa and 394 MPa, respectively. Notch tensile strength of the unwelded parent metal and FSW joints are 571 MPa and 410 MPa, respectively. This indicates that there is a 30% reduction in tensile strength due to FSW process.

Table 3 Transverse tensile properties of parent metal and FSW joint

Material	Parent metal	FSW joint
Yield strength/MPa	510	335
Ultimate tensile strength/MPa	563	394
Elongation in 50 mm gauge length/%	16	12
Notch tensile strength/MPa	571	410
Notch strength ratio (NSR)	1.01	1.04
Joint efficiency/%	−	70

3.3 Microstructure

Figure 6 shows the micrographs of parent metal and FSW joint. The optical macrograph of the defect-free weld joint which defines all the zones of the FSW joint is shown in Fig. 6(a). Figure 6(b) shows the optical microstructure of parent metal consisting of very fine insoluble second phase precipitates dispersed in various locations of elongated grain. The microstructure of the welded joint was normally divided into the following three regions: the dynamically recrystallized zone (DXZ) or the weld nugget, thermo-mechanically affected zone

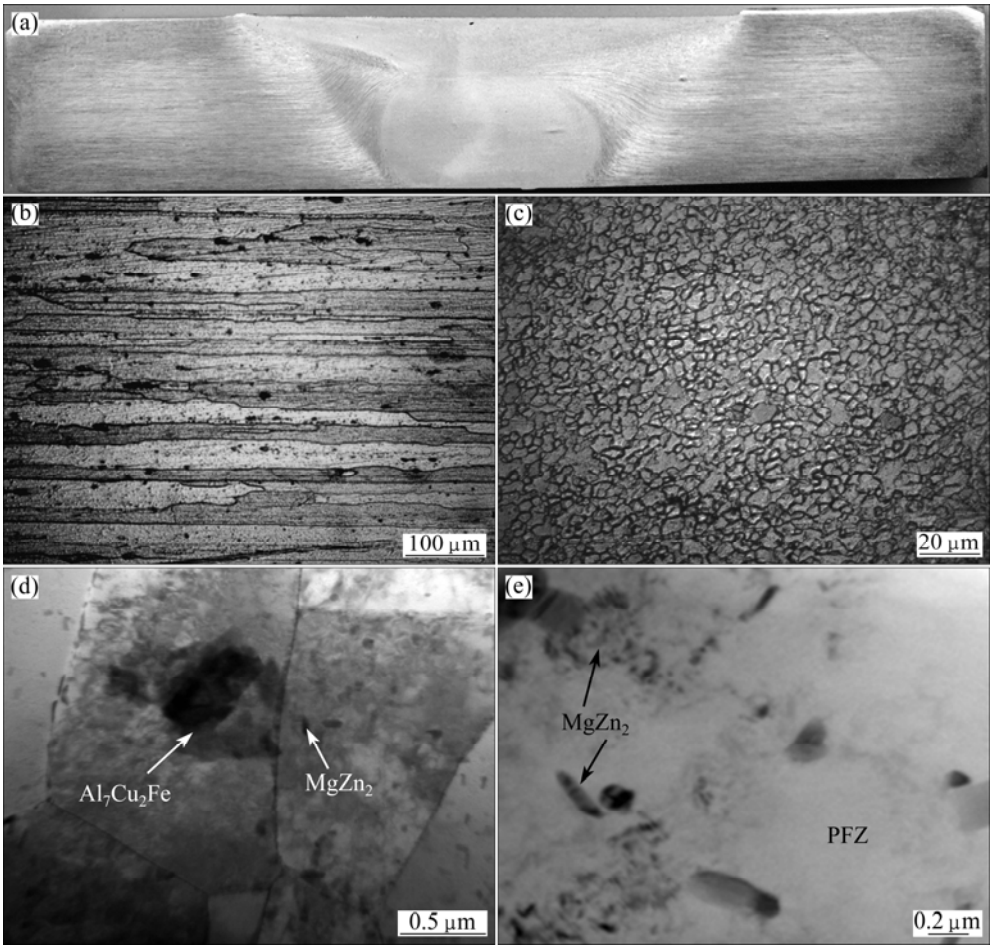

Fig. 6 Photographs of parent metal and FSW joint: (a) Macrograph of optimized weld joint; (b) OM image of parent metal; (c) OM image of stir zone (near crack tip); (d) TEM image of parent metal; (e) TEM image of stir zone

(TMAZ), and heat-affected zone (HAZ) [20]. Figure 6(c) represents the microstructure of middle zone of the nugget. The middle zone microstructure is finer compared with parent metal. The microstructure was partially recrystallized, with fairly large recrystallized grains that were flattened and elongated in the longitudinal direction as a consequence of the mechanical deformation introduced by the rolling operation. The recrystallized grain size was non-uniform along each of the three orthogonal directions of the wrought plate, resulting in an anisotropic microstructure. The weld nugget is characterized by a recrystallized, fine equiaxed grain structure because the precipitates have fully or partially gone into solution and re-precipitated during the joining process. The transition zone between the HAZ and the weld nugget is TMAZ characterized by a highly deformed structure [21]. The pre-crack is initiated in the weld nugget only. So, in this article only weld nugget zone microstructure was discussed. The weld nugget is composed of fine- equiaxed recrystallized grains, which are formed under the high temperature and high rate of deformation in the weld nugget due to the pins stirring [22], and the size of the crystal grain is very fine. The TEM image of PM (Fig. 6(d)) shows the coarse elongated grains of the as-received AA7075 aluminum alloy plate which is oriented parallel to the rolling direction. It also consists of coarse Al_7Cu_2Fe and finer $MgZn_2$ strengthening precipitates. In FSW joint, the finer precipitates which are the major strengthening precipitates are completely dissolved in the matrix and very few coarser particles (Al_7Cu_2Fe) which are broken down during the FSW are seen in Fig. 6(e).

3.4 Microhardness

The hardness across the weld cross section was measured along the mid thickness of the joint using a Vickers microhardness testing machine. The unwelded parent metal shows hardness of HV155 and the hardness was lowered to HV 143 at the stir zone. Figure 7 shows the hardness profile which is basin like profile indicating that the stir zone undergoes softening due to the heat supplied by the FSW process.

3.5 Fractography

Figure 8 shows the various regions of fracture surface of PM and friction stir zone. Figures 8(a) and (b) show the scanned images of fracture surface of PM and friction stir zone at low magnification. The SEM images of fatigue crack initiation (FCI) region of PM and FSZ are shown in Figs. 8(c) and (d) respectively. The SEM images of fatigue crack propagation (FCP) region of PM and FSZ are shown in Figs. 8(e) and (f) respectively. The SEM images of final failure region (FF) region of PM and FSZ are shown in Figs. 8(g) and (h) respectively. The SEM fractograph of FCI region clearly depicts the existence of fine dimples. While in FSW joint, the fractograph of FCI region shows the tear lips like features. This is due to the stirred region consisting of very fine irregular grains. Stage I fatigue fracture surfaces is faceted, often resemble cleavage, and does not exhibit fatigue striations. Stage I fatigue is normally observed on high-cycle low-stress fractures and is frequently absent in low-cycle high-stress fatigue.

Invariably in both PM (Fig. 8(e)) and FSW joint (Fig. 8(f)), the fracture surface shows the crack arrest marks known as fatigue striations, which are the visual record of the position of the fatigue crack front during crack propagation through the material. The PM fractograph shows the presence of striations in the facets itself. This can be adjudged by the characteristic feature

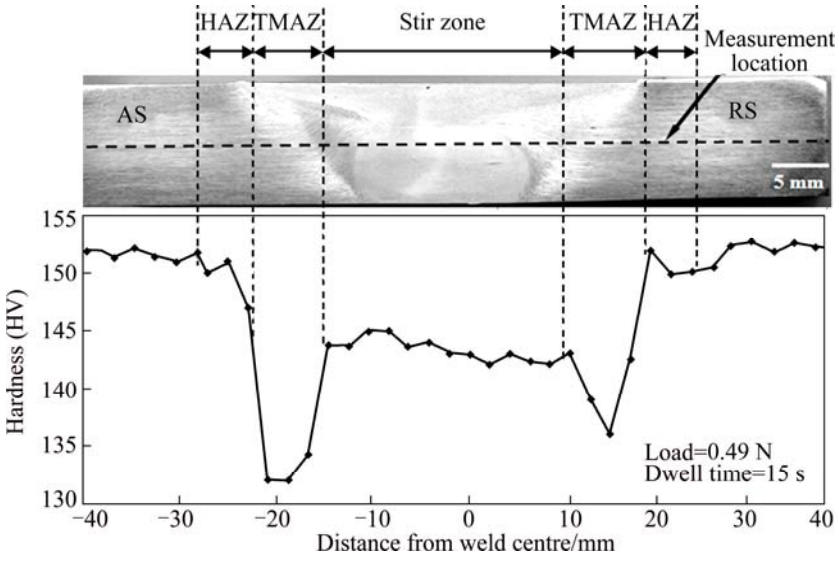

Fig. 7 Hardness profile along mid thickness

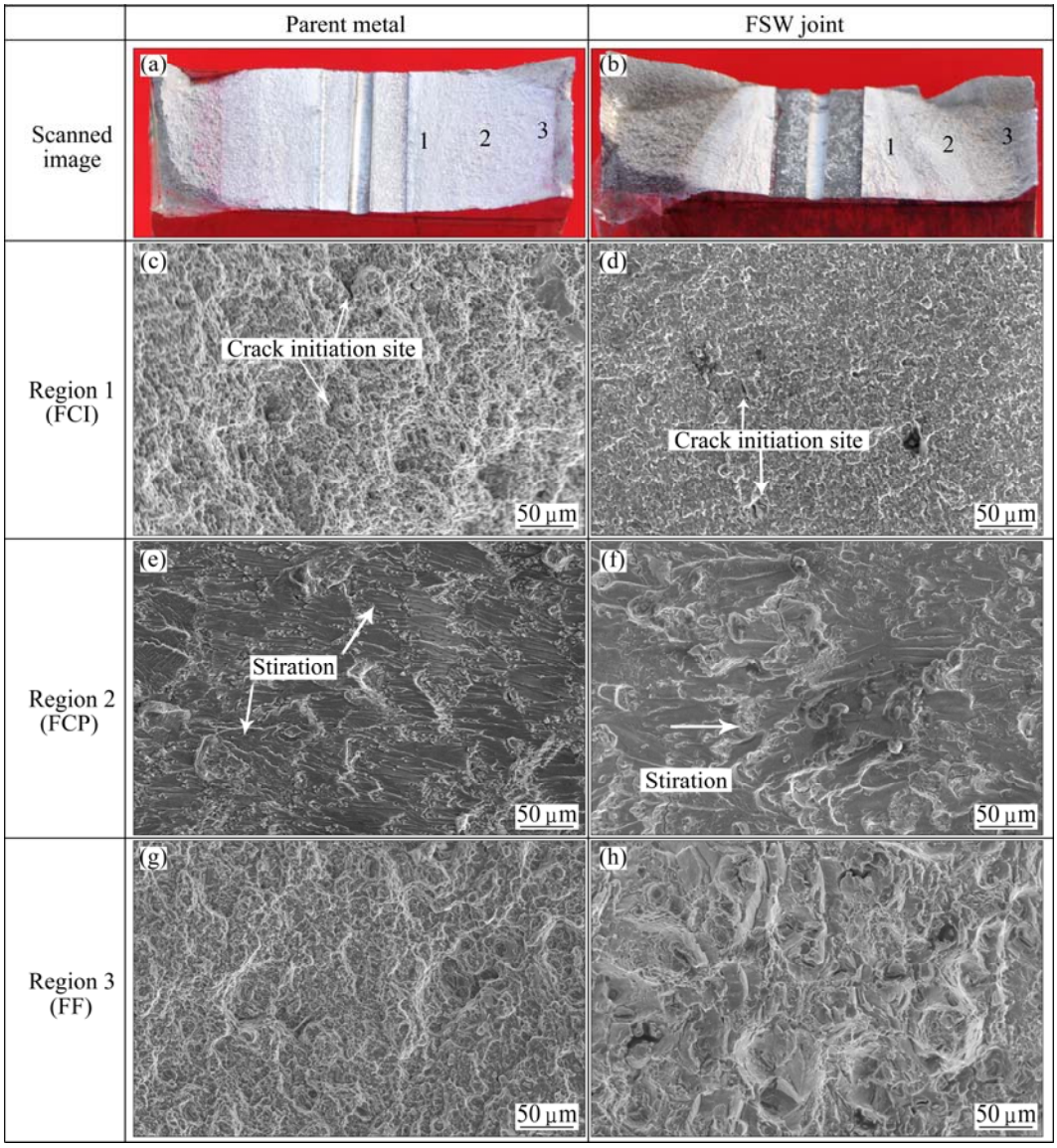

Fig. 8 SEM fractographs of different fatigue crack growth regions of parent metal and FSW

of the fatigue striations. The striations are parallel and right angles to the local direction of crack propagation. In FSW joint fractograph (Fig. 8(f)), the change from transgranular facets to dimples like fracture surface can be easily visible. From the FCP region fractograph, it is understood that the spacing between striations is wider in FSW joint, closer in PM.

Figure 8(g) exhibits the fracture surface appearance of final failure region region (where unstable crack growth occurred) of PM. From the fractograph it is observed that the tear dimples are elongated along the loading direction and this is mainly because of the limit load condition at the time of final fracture. Even though unstable crack growth occurred in the final failure region, the final fracture took place in the ductile mode and it is evident in the presence of fine dimples. The modes of failure for the final failure region of PM and the welded joints are a combination of ductile with microvoid coalescence. In this FSW joint fractograph, facets are the dominant failure patterns, but in PM fractograph and dimples are more predominant, which is clearly visible from the fractograph. To summarize, the final fracture surface of base metal contains only dimples; higher amount of facets and less area of dimples (both facets and dimples) are observed in FSW joint. This suggests that the resistance offered by PM against the growing fatigue crack, even in the unstable crack growth region, is much better than FSW joint.

4 Discussion

From the fatigue crack growth test results (Table 3), it is understood that the parent metal has superior fatigue crack growth resistance compared with FSW joints. The

fatigue crack growth exponent was obtained from the slope of the curve drawn between da/dN and ΔK range. If this exponent is higher, then the slope of the curve is higher, indicating the resistance offered by the material to the growing fatigue crack is lower and hence the fatigue life will be shorter and vice versa. The reasons for the poor fatigue crack growth resistance of the FSW joint compared with the parent material are inferior tensile properties of the joints. The lower elongation in the FSW joint imparts lower resistance to the fatigue crack growth and hence higher fatigue crack growth rate is observed in FSW joint compared to the parent material [2].

It is a general tendency that the fatigue crack growth resistance simply becomes greater as the tensile strength or the yield strength obtained from the static tensile test becomes greater, because the plastic strain per load cycle is reduced [23]. The yield strength has a major influence on the fatigue crack behaviour of FSW joint. Lower yield strength and lower microhardness of the FSW joint resulted in inferior fatigue crack growth resistance compared to the parent metal.

Reduction in elongation (lower ductility) of the FSW joint also imparts lower resistance to fatigue crack propagation and hence fatigue crack growth rate is relatively high compared to the parent metal. The combined effect of higher yield strength and higher ductility of the parent metal enhanced resistance to crack initiation and crack propagation and hence the fatigue performance of the parent metal is superior compared with FSW joints.

The microstructure of the weld region (stir zone) also plays a major role in deciding the properties of friction stir welded AA7075-T651 alloy. Mechanical properties of FSW joints depend on structural characteristics of weld region, which in turn depends on the specific thermal/mechanical cycles imposed during friction stir welding. Fine equiaxed grains in the stir zone imply that dynamic recrystallization has taken place during welding due to plastic deformation at elevated temperature. In heat treatable alloys, the static properties of the friction stir welds are dependent on the distribution of strengthening precipitates rather than the grain size [24].

The size and distribution of $CuAl_2$ precipitates play a major role in deciding the tensile properties and microhardness of FSW joints. The frictional heat and mechanical working of the plasticized material in the stir zone result in coarse and agglomerated precipitates in some areas and precipitate free zone (PFZ) due to dissolution of precipitates in the stir zone. This leads to considerable softening in contrast to the base metal. This decreases the hardness of stir zone in FSW joint considerably and resulted in lower tensile strength as well as fatigue crack growth resistance than the parent metal. Generally, fine and uniformly distributed $CuAl_2$ precipitates hinder the growth of the fatigue crack. Dissolution of $CuAl_2$ precipitate in the stir zone resulted in lower fatigue crack growth resistance due to reduced obstacle for the growing crack [25]. Hence, from the above discussion it can be concluded that inferior tensile properties, reduced hardness, dissolution of $CuAl_2$ precipitates are the main reasons for lower fatigue crack growth resistance of FSW joint compared with its parent metal.

5 Conclusions

Fatigue crack growth resistance of friction stir welded AA7075-T651 alloy joint is appreciably lower than that of the unwelded parent metal. Though friction stir welding produces recrystallized finer grains at the stir zone, the yield strength, notch tensile strength and hardness are lower. This may be due to the dissolution of precipitates during friction stir welding which needs further investigation.

Acknowledgements

The authors would like to thank Dr. A. K. LAKSHMINARAYANAN, associate professor, SSN college of Engineering, Chennai, India for providing technical support to carry out this investigation. The first two authors are grateful to the Centre for Materials Joining & Research (CEMAJOR), Department of Manufacturing Engineering, Annamalai University, for extending all the necessary facilities to carry out this investigation.

References

[1] RAVINDRA B, SENTHIL KUMAR T, BALASUBRAMANIAN V. Fatigue life prediction of gas metal arc welded cruciform joints of AA7075 aluminium alloy failing from root region [J]. Transactions of Nonferrous Metals Society of China, 2011, 21(6): 1210−1217.

[2] BALASUBRAMANIAN V, RAVISANKAR V, MADHUSUDHAN REDDY G. Effect of post weld aging treatment on fatigue behaviour of pulsed current welded AA7075 aluminium alloy joints [J]. Materials Engineering and Performance, 2008, 7(2): 224−233.

[3] FENG A H, CHEN D L, MA Z Y. Microstructure and cyclic deformation behavior of a friction-stir-welded 7075 Al alloy [J]. Metallurgical and Materials Transactions A, 2010, 41: 957−971.

[4] MADHUSUDHAN REDDY G, GOKHALE A A, PRASAD RAO K. Weld microstructure refinement in a 1441 grade aluminium−lithium alloy [J]. Materials Science, 1997, 32: 4117−4126.

[5] GENEVOIS C, DESCHAMPS A, DENQUIN A, DOISNEAU-COOTTIGNIES B. Quantitative investigation of precipitation and mechanical behaviour for AA2024 friction stir welds [J]. Acta Materialia, 2005, 53: 2447−2458.

[6] SCIALPI A, de FILIPPIS L A C, CAVALIERE P. Influence of shoulder geometry on microstructure and mechanical properties of

friction stir welded 6082 aluminium alloy [J]. Materials and Design, 2007, 28(4): 1124−1129.

[7] SUTTON M A, REYNOLDS A P, WANG D Q, HUBBARD C R. A study of residual stresses and microstructure in 2024-T3 aluminum friction stir butt welds [J]. Engineering Materials and Technology, 2002, 124: 215−222.

[8] HASSAN A A, NORMA A F, PRICE D A, PRANGNELL P B. Stability of nugget zone grain structures in high strength Al-alloy friction stir welds during solution treatment [J]. Acta Materialia, 2003, 51(7): 1923−1936.

[9] MOREIRA P M G P, SANTOS T, TAVARES S M O, RICHTER-TRUMMER V, VILAÇA P, de CASTRO P M S T. Mechanical and metallurgical characterization of friction stir welding joints of AA6061-T6 with AA6082-T6 [J]. Materials and Design, 2009, 30(1): 180−187.

[10] MALARVIZHI S, BALASUBRAMANIAN V. Fatigue crack growth resistance of gas tungsten arc, electron beam and friction stir welded joints of AA2219 aluminium alloy [J]. Materials and Design, 2011, 32: 1205−1214.

[11] CHEN Jun-zhou, ZHEN Liang, YANG Shou-jie. Effects of precipitates on fatigue crack growth rate of AA 7055 aluminum alloy [J]. Transactions of Nonferrous Metals Society of China, 2010, 20: 2209−2214.

[12] ZHAO Tian-wen, JIANG Yan-yao. A study of fatigue crack growth of 7075-T651 aluminum alloy [J]. International Journal of Fatigue, 2008, 30: 834−849.

[13] ZHOU Cai-zhi, YANG Xin-qi, LUAN Guo-hong. Fatigue properties of friction stir welds in Al 5083 alloy [J]. Scripta Materialia, 2005, 53: 1187−1191.

[14] CAVALIERE P, de SANTIS A, PANELLA F, SQUILLACE A. Effect of anisotropy on fatigue properties of 2198 Al−Li plates joined by friction stir welding [J]. Engineering Failure Analysis, 2009, 16: 1856−1865.

[15] SRIVATSAN T S, ANAND S, SRIRAM S, VASUDEVAN V K. The high-cycle fatigue and fracture behavior of aluminium alloy 7055 [J]. Materials Science and Engineering A, 2000, 281: 292−304.

[16] LAKSHMINARAYANAN A K, BALASUBRAMNAIAN V. The mechanical properties of the GMAW, GTAW and FSW joints of the RDE-40 aluminium alloy [J]. Microstructure and Materials Properties, 2008, 3(6): 837−853.

[17] DIETER G E. Mechanical metallurgy [M]. New York: McGraw-Hill Publishers, 1988: 376−431.

[18] HELLAN K. Introduction to fracture mechanics [M]. New York: McGraw Hill Publishers, 1983: 172−173.

[19] SONSINO C M. Fatigue assessment of welded joints in Al−Mg−4.5Mn aluminium alloy AA 5083 by local approaches [J]. International Journal of Fatigue, 1999, 21: 985−999.

[20] LIU H J, FUJII H, MAEDA M, NOGI K. Heterogeneity of mechanical properties of friction stir welded joints of 1050-H24 aluminum alloy [J]. Journal of Materials Science Letters, 2003, 22: 441−444.

[21] SINGH R K R, SHARMA C, DWIVEDI D K, MEHTA N K, KUMAR P. The microstructure and mechanical properties of friction stir welded Al−Zn−Mg alloy in as welded and heat treated conditions [J]. Materials and Design, 2011, 32: 682−687.

[22] JATA K V, SEMIATIN S L. Continuous dynamic recrystallization during friction stir welding of high strength aluminium alloys [J]. Scripta Materialia, 2000, 43(8): 743−749.

[23] LAKSHMINARAYANAN A K, BALASUBRAMANIAN V. Assessment of fatigue life and crack growth resistance of friction stir welded AISI 409M ferritic stainless steel joints [J]. Materials Science and Engineering A, 2012, 53(9): 143−153.

[24] MOATAZ ATTALLAH M, HANADI SALEM G. Friction stir welding parameters: A tool for controlling abnormal grain growth during subsequent heat treatment [J]. Material Science and Engineering A, 2004, 391(1−2): 51−59.

[25] MADHUSUDHAN REDDY G, MASTANAIAH P, SATA PRASAD K, MOHANDAS T. Microstructure and mechanical property correlation in AA 6061 aluminium alloy friction stir weld [J]. Transactions of the Indian Institute of Metals, 2009, 62(1): 49−58.

搅拌摩擦焊 AA7075-T651 铝合金接头的疲劳裂纹扩展

P. SIVARAJ, D. KANAGARAJAN, V. BALASUBRAMANIAN

Department of Manufacturing Engineering, Annamalai University, Annamalai Nagar, Tamil Nadu 608002, India

摘　要：研究 12 mm 厚 AA7075-T651 铝合金板搅拌摩擦焊接头的疲劳裂纹扩展行为。从搅拌摩擦焊接头以及母材中截取试样，对试样进行疲劳裂纹扩展实验。对搅拌摩擦焊接头以及母材的横向拉伸性能进行评估。用光学显微镜和透射电镜分析焊接接头的显微组织。用扫描电镜观察试样的断裂表面。与母材相比，焊接接头的 ΔK_{cr} 降低了 10×10^{-3} MPa·m$^{1/2}$。搅拌摩擦焊 AA7075-T651 接头的疲劳寿命明显低于母材的，其原因可归结于焊缝区的析出相在搅拌摩擦焊接过程中的溶解。

关键词：AA 7075 铝合金；搅拌摩擦焊；疲劳裂纹扩展；显微组织

(Edited by Hua YANG)